Kinetic plasma waves carrying orbital angular momentum

D. R. Blackman,[1] R. Nuter,[1] Ph. Korneev,[2,3] and V. T. Tikhonchuk[1,4]
[1]*CELIA, University of Bordeaux, CNRS, CEA, F-33405 Talence, France*
[2]*National Research Nuclear University "MEPhI" (Moscow Engineering Physics Institute), Moscow 115409, Russia*
[3]*P. N. Lebedev Physics Institute, Russian Academy of Sciences, 119991 Moscow, Russia*
[4]*ELI-Beamlines, Institute of Physics, Czech Academy of Sciences, 25241 Dolní Břežany, Czech Republic*

(Received 25 March 2019; published 15 July 2019)

The structure of Langmuir plasma waves carrying a finite orbital angular momentum is revised in the paraxial approximation. It is shown that the kinetic effects related to higher-order momenta of the electron distribution function lead to coupling of Laguerre-Gaussian modes and result in a modification of the wave dispersion and damping. The theoretical analysis is compared to the three-dimensional particle-in-cell numerical simulations for a mode with orbital momentum $l = 2$. It is demonstrated that propagation of such a plasma wave is accompanied with generation of quasistatic axial and azimuthal magnetic fields which result from the orbital and longitudinal momenta transported with the wave, respectively.

DOI: 10.1103/PhysRevE.100.013204

I. INTRODUCTION

It was discussed in the seminal paper by Allen *et al.* [1] that electromagnetic waves may carry orbital angular momentum (OAM), while propagating in vacuum, which can be transferred to particles if the wave is absorbed. This feature has found various applications in optics for compact storing of information, nanoscale imaging, and manipulation [2]. Mathematically such beams are presented with Laguerre-Gaussian functions, which are eigenmodes of the paraxial optics equation in the cylindrical coordinates. Recent publications show the potential applications of OAM modes in particle focusing and acceleration, generation of strong plasma waves, wake-field excitation, and quasistatic magnetic fields [3–6].

Propagation of OAM optical beams in plasmas is associated with excitation of plasma waves that may also carry orbital momentum [7]. The study of these waves is of particular interest as they are coupled to plasma electrons and are involved in such processes as Landau damping and particle acceleration. The kinetic plasma waves in the cylindrical geometry have been studied by Mendonça [8]. In contrast to common plasma waves these "twisted plasmons" demonstrate different dispersion and damping properties. However, the development of the wave dispersion equation in Ref. [8] suffers from some inconsistencies and properties of these twisted modes, including the dispersion relation and the damping rate, are not faultlessly analyzed. The present paper is dedicated to a more detailed and consistent analysis of the twisted kinetic plasma waves. It is shown that because of direct coupling of plasma wave electric field to particles, the Laguerre-Gaussian (LG) functions are not the eigenfunctions of the electron kinetic equation. While the Poisson equation for the plasma wave electric field can be developed in a series of LG functions, these LG functions are coupled in the electron kinetic equation because of the electron motion in the radial and azimuthal direction. This coupling can be treated by using an expansion on the paraxial parameter—the ratio of the plasma wavelength to the radial width of the wave packet—which is supposed to be small. By the presented analysis, the dispersion properties of the twisted plasmons are shown to be strongly mode dependent in certain parameter ranges.

An additional area of interest is the generation of quasistatic magnetic field on the second order of the amplitude of the plasmon. This phenomenon was previously observed in simulations described in Ref. [9] where two co-propagating OAM laser pulses with differing angular mode, frequency, and wavelength are injected into a plasma and couple with an OAM plasmon. The resulting plasmon is shown to generate a second-order quasistatic magnetic field. The distribution function obtained in the analysis performed here is used to calculate the second-order magnetic field. The resulting field structure is significantly more complex than the field described in Ref. [9]; we also present numerical results which match the theoretical predictions made here.

In what follows we briefly recall the representation of the paraxial optics wave equation in a series of LG functions and apply the same approach to electron plasma wave equation. It is shown that the modes with different radial and azimuthal wave numbers are coupled to each other, so no definite angular momentum can be associated with a plasma wave. However, in the paraxial approximation, where the plasma wavelength is much smaller than the transverse size of the wave beam, only the coupling between neighboring modes can be retained and the dispersion equation can be presented in a closed form.

The analysis of this dispersion equation in several particular cases provides the examples of the specific evolution of twisted plasma waves and their coupling to plasma particles. The analytical results are compared and illustrated with three dimensional numerical simulations.

II. DISPERSION EQUATION FOR THE PLASMA WAVE IN A CYLINDRICAL GEOMETRY

A. LG modes in optics

An electric field $\mathbf{E}$ of the electromagnetic wave propagating in vacuum along the z axis can be represented in an envelope approximation as

$$\mathbf{E} = \mathbf{e}\, E_0(\tau)\, \exp(-i\omega t + ikz)\, U(z, r, \theta), \tag{1}$$

where $\mathbf{e}$ is the constant polarization unitary vector, ω is the wave frequency, $k = \omega/c$ is the axial wave number, $\tau = t - z/c$ is the co-propagating time, $E_0(\tau)$ is the slowly changing in time amplitude, and a scalar function U is describing the waveform in the transverse plane, with r, θ, and z being the radial, azimuthal, and longitudinal components. It is a solution of the paraxial wave equation,

$$(2ik\partial_z + \nabla_\perp^2)\, U = 0, \tag{2}$$

where the second derivative in z is neglected assuming that function U evolves slowly in the propagation direction. In the cylindrical geometry the function U can be developed in a series of eigenmodes, which are the LG functions:

$$U(z, r, \theta) = \sum_{p,l} c_{p,l} F_{p,l}(X)\, \exp\left(il\theta + i\varphi_{p,l} + \frac{ikr^2}{2f}\right). \tag{3}$$

Here $X = r^2/w_b^2$ is the normalized radial coordinate, $w_b(z) = w_{b,0}\sqrt{1 + z^2/z_R^2}$ is the beam radius, for brevity $w_b(z)$ is referred to as w_b throughout the text, $w_{b,0}$ is the beam waist at the focal point, $z_R = k w_{b,0}^2$ is the Rayleigh length, $\varphi_{p,l}(z) = -(2p + |l| + 1)\arctan(z/z_R)$ is the Gouy phase, $f(z) = z + z_R^2/z$ is the wavefront curvature, and $c_{p,l}$ is a constant coefficient. The radial wave number $p \geqslant 0$ is an integer that numerates radial modes. The integer l could be positive or negative, and it numerates the orbital angular momentum (OAM).

The eigenfunction $F_{p,l}$ is the LG mode:

$$F_{p,l}(X) = \sqrt{\frac{p!}{(|l| + p)!}} X^{|l|/2} L_p^{|l|}(X)\, e^{-X/2}, \tag{4}$$

where $L_p^{|l|}(X)$ is a generalized, or associated, Laguerre polynomial of degree p and l which may be defined by the Rodriguez representation [10]:

$$L_p^l(x) = (p!)^{-1} e^x x^{-l} d_x^p (e^{-x} x^{l+p}). \tag{5}$$

The set of functions $F_{p,l}$ are orthogonal and normalized according to the following relation:

$$\int_0^\infty dX\, F_{p,l}(X)\, F_{p',l}(X) = \delta_{p,p'}, \tag{6}$$

where $\delta_{p,p'}$ is the symbol of Kronecker. The orthogonality on different angular momenta l and l' is assured by the factor $e^{il\theta}$ in Eq. (3). The eigenfunctions $F_{p,l}$ do not depend on the sign of the OAM.

So a relatively simple and compact representation of the OAM beam in optics in vacuum, or in a dielectric medium without spatial dispersion, originates from Eq. (2), the Laplacian in the transverse plane comes from Maxwell's equations. Presentation of the wave field in a series of LG functions (3) is valid if the paraxial parameter is sufficiently small, $1/k w_{b,0} \ll 1$. Application of the same approach to the electrostatic electron plasma wave is presented in the next section.

B. LG modes presentation for the plasma wave

We consider a small amplitude plasma wave in a constant density plasma described by the electrostatic potential Φ and the electron distribution function f_e. The potential satisfies the Poisson equation,

$$\Delta\Phi = \frac{e}{\epsilon_0}\, \delta n_e, \tag{7}$$

where e is the electron charge, ϵ_0 is the vacuum dielectric permittivity, and $\delta n_e = \int d\mathbf{v}\, \delta f_e$ is the perturbation of the electron density. The potential Φ is related to the deviation of the electron distribution function $\delta f_e = f_e - f_{e0}$ from the equilibrium Maxwellian distribution,

$$f_{e0}(\mathbf{r}, \mathbf{v}, t) = n_{e0}(2\pi T_e/m_e)^{-3/2} \exp(-\varepsilon/T_e), \tag{8}$$

which is characterized by the density n_{e0}, temperature T_e, electron energy $\varepsilon = m_e \mathbf{v}^2/2$, and the electron mass m_e.

For a monochromatic plasma wave, with the frequency ω and wave number k, we are looking for solutions to the Poisson equation (7) and the linearized Vlasov kinetic equation in the paraxial approximation, $1/k w_{b,0} \ll 1$. Following the standard approach which was already applied for the twisted plasma waves in Ref. [8], we represent the solution of this system as a series of LG functions:

$$\Phi(z, r, \theta, t) = \sum_{p,l} \phi_{p,l} F_{p,l}(X) \times \exp(-i\omega t + ikz + il\theta + i\varphi_{p,l} + iqX), \tag{9}$$

$$\delta f_e(z, r, \theta, \mathbf{v}, t) = \sum_{p,l} f_{p,l}(\mathbf{v}) F_{p,l}(X) \times \exp(-i\omega t + ikz + il\theta + i\varphi_{p,l} + iqX), \tag{10}$$

where $q = k w_b^2/2f = z/2z_R$ is the factor accounting for the front curvature. Similar to the use of the solution set shown by Eq. (3) to solve Eq. (2), we use the set of Eqs. (9) and (10) to solve the Poisson equation in the paraxial approximation:

$$k^2\Phi = -\frac{e}{\epsilon_0} \int d\mathbf{v}\, \delta f_e. \tag{11}$$

It results in a system of algebraic equations for the potential amplitudes $\phi_{p,l}$ and partial distribution functions $f_{p,l}(\mathbf{v})$. The Poisson equation (11) is linear, it thus provides relations between the coefficients of the same mode:

$$\phi_{p,l} = -\frac{e}{\epsilon_0 k^2} \int d\mathbf{v}\, f_{p,l}. \tag{12}$$

The situation is more complicated with the Vlasov equation, which does not separate into a set of independent equations because the gradient operators $v_z\partial_z$ and $\mathbf{v}_\perp \cdot \nabla_\perp$ couple the modes with different orbital momenta and radial structure.

The axial derivative can be presented as follows:

$$e^{-i\varphi_{p,l}-iqX}v_z\partial_z e^{i\varphi_{p,l}+iqX}F(X) = -(2p+|l|)\frac{iv_z}{kw_b^2}F + \frac{iv_z}{2kw_b^2}XF - \frac{v_z}{kw_b^2}XF',$$

where $F' = dF/dX$. All the terms in the right-hand side are of the second order over the paraxial parameter $1/kw_b$ with respect to the dominant term ikv_zF. These second-order terms are neglected in our analysis. Then the kinetic equation reads

$$-i(\omega - kv_z)\,\delta f_e + \mathbf{v}_\perp\cdot\nabla_\perp\delta f_e = -iekv_z\Phi\,\partial_\varepsilon f_{e0} - e\mathbf{v}_\perp\cdot\nabla_\perp\Phi\partial_\varepsilon f_{e0}, \tag{13}$$

where the expression $\partial_{\mathbf{v}} f_{e0} = m_e\mathbf{v}\partial_\varepsilon f_{e0}$ is used for the derivative of the electron distribution function assuming that it depends only on the electron energy. The operator of differentiation on transverse coordinates can be calculated as follows:

$$\begin{aligned}e^{-iqX}\mathbf{v}_\perp\cdot\nabla_\perp e^{il\theta+iqX}F(X) &= e^{-iqX}\left[v_\perp\cos(\theta-\theta_v)\,\partial_r - \frac{v_\perp}{r}\sin(\theta-\theta_v)\,\partial_\theta\right]e^{il\theta+iqX}F(X)\\ &= \frac{v_\perp}{w_b}e^{i(l+1)\theta-i\theta_v}\sqrt{X}F' + \frac{v_\perp}{w_b}e^{i(l-1)\theta+i\theta_v}\sqrt{X}F' - iq\frac{v_\perp}{w_b}e^{i(l+1)\theta-i\theta_v}\sqrt{X}F + iq\frac{v_\perp}{w_b}e^{i(l-1)\theta+i\theta_v}\sqrt{X}F\\ &\quad - \frac{l}{2\sqrt{X}}\frac{v_\perp}{w_b}e^{i(l+1)\theta-i\theta_v}F + \frac{l}{2\sqrt{X}}\frac{v_\perp}{w_b}e^{i(l-1)\theta+i\theta_v}F.\end{aligned}$$

Here $v_r = v_\perp\cos(\theta-\theta_v)$ and $v_\theta = -v_\perp\sin(\theta-\theta_v)$ are the radial and azimuthal components of electron velocity and θ_v is the angle of the electron velocity in the transverse plane. By using the properties of the Laguerre functions [10], the derivative of the function F can be expressed as

$$\sqrt{X}\,F'_{p,l}(X) = \frac{1}{2}\sqrt{p+1}F_{p+1,l-1}(X) - \frac{1}{2}\sqrt{p}F_{p-1,l+1}(X). \tag{14}$$

See Appendix A for details. By multiplying Eq. (13) by the factor $F_{p',l'}\exp(-il'\theta - iqX)$ and performing integration over the transverse coordinates, one obtains the following system of algebraic equations for the coefficients $f_{p,l}$:

$$(\omega - kv_z)\,f_{p,l} + i\sum_{p',l'}M_{p,l;p',l'}f_{p',l'} = ekv_z\phi_{p,l}\partial_\varepsilon f_{e0} - ie\sum_{p',l'}M_{p,l;p',l'}\phi_{p',l'}\partial_\varepsilon f_{e0}, \tag{15}$$

where the matrix elements $M_{p,l;p',l'}$ are defined as follows:

$$M_{p,l;p',l'} = \frac{1}{\pi w_b^2}\int_0^{2\pi}d\theta\int_0^\infty dr\,r\,F_{p,l}(X)e^{-il\theta-iqX}\,\mathbf{v}_\perp\cdot\nabla_\perp e^{il'\theta+iqX}F_{p',l'}(X). \tag{16}$$

Performing the integrations in Eq. (16) one finds the following expression for the matrix elements:

$$M_{p,l;p',l'} = \frac{v_\perp}{w_b}[e^{-i\theta_v}\delta_{l,l'+1}K^-_{p,l;p',l'} + e^{i\theta_v}\delta_{l,l'-1}K^+_{p,l;p',l'}]. \tag{17}$$

The matrices K^+ and K^- describe coupling of the modes with neighboring orbital moments:

$$\begin{aligned}K^\mp_{p,l;p',l'} = \frac{\exp[i(\varphi_{p',l'}-\varphi_{p,l})]}{2}\int_0^\infty dX\,F_{p,l}(X)\Big[&\sqrt{p'+1}\,F_{p'+1,l'-1}(X) - \sqrt{p'}\,F_{p'-1,l'+1}(X)\\ &+ \frac{iz}{z_R}\sqrt{X}\,F_{p',l'}(X) \mp \frac{l'}{\sqrt{X}}F_{p',l'}(X)\Big].\end{aligned} \tag{18}$$

Considering Eq. (15) one can see the principal difference from the study presented in Ref. [8], where couplings between the neighboring orbital modes were neglected and the operator $\mathbf{v}_\perp\cdot\nabla_\perp$ was replaced by its average value for each mode separately. This set of equations can be further simplified by developing the elements of the electron distribution function in Fourier series of the velocity angle:

$$f_{p,l}(\theta_v) = \sum_m f^{(m)}_{p,l}e^{-im\theta_v}.$$

Then by integrating Eq. (15) over the azimuthal velocity angle θ_v one obtains a series of equations for the moments of the partial distribution function $f^{(m)}_{p,l}$:

$$\begin{aligned}&(\omega - kv_z)\,f^{(m)}_{p,l} + i\frac{v_\perp}{w_b}\sum_{p'}\left[K^-_{p,l;p',l-1}f^{(m-1)}_{p',l-1} + K^+_{p,l;p',l+1}f^{(m+1)}_{p',l+1}\right]\\ &\quad = ekv_z\phi_{p,l}\delta_{m,0}\partial_\varepsilon f_{e0} - ie\frac{v_\perp}{w_b}\sum_{p'}[K^-_{p,l;p',l-1}\phi_{p',l-1}\delta_{m,1} + K^+_{p,l;p',l+1}\phi_{p',l+1}\delta_{m,-1}]\partial_\varepsilon f_{e0}.\end{aligned} \tag{19}$$

Along with Eq. (12), which includes the function $f^{(0)}_{p,l}$, this system fully defines linear plasma waves with arbitrary orbital momentum. The LG modes are coupled both in orbital momentum l to close neighbors and in radial number p in the first order on the paraxial parameter.

C. Dispersion equation for the twisted plasma wave

The system of Eqs. (12) and (19), obtained in the paraxial approximation ($1/kw_b \ll 1$), could be further simplified. The paraxial approximation implies smallness of the mode-coupling terms. Thus, the equation for $f^{(0)}_{p,l}$ in (19) can be simplified by accounting for coupling to $f^{(\pm1)}_{p,l}$ but neglecting the higher-order harmonics. Then, the equations for the first harmonics read

$$(\omega - kv_z) f^{(\pm1)}_{p,l} = -i\frac{v_\perp}{w_b}\sum_{p'} K^{\mp}_{p,l;p',l\mp1} \times \left(f^{(0)}_{p',l\mp1} + e\phi_{p',l\mp1}\partial_\varepsilon f_{e0}\right). \quad (20)$$

Substituting this expression into Eq. (19) for the harmonic $f^{(0)}_{p,l}$ one finds

$$f^{(0)}_{p,l} = e\frac{kv_z}{\omega - kv_z}\phi_{p,l}\partial_\varepsilon f_{e0} - \frac{v_\perp^2}{w_b^2}\frac{1}{(\omega - kv_z)^2}\sum_{p'} Q^{(l)}_{p,p'}\left(f^{(0)}_{p',l} + e\phi_{p',l}\partial_\varepsilon f_{e0}\right), \quad (21)$$

where the notation for the mode-coupling coefficient is introduced:

$$Q^{(l)}_{p,p'} = \sum_{p''\geqslant 0}[K^{-}_{p,l;p'',l-1}K^{+}_{p'',l-1;p',l} + K^{+}_{p,l;p'',l+1}K^{-}_{p'',l+1;p',l}]. \quad (22)$$

The second term in the right-hand side of Eq. (21) contains the dominant term with $p' = p$ and all other terms with $p' \neq p$ are of the second order. By retaining the first-order terms one obtains the final expression for $f^{(0)}_{p,l}$:

$$f^{(0)}_{p,l} = \left[-1 + \frac{\omega(\omega - kv_z)}{(\omega - kv_z)^2 + Q^{(l)}_{p,p}v_\perp^2/w_b^2}\right] e\phi_{p,l}\partial_\varepsilon f_{e0}. \quad (23)$$

In the second term, it is important to account for the second-order term in the denominator, which shifts the resonance condition $\omega = kv_z$ due to the transverse structure of the plasma wave. By substituting this expression for the electron distribution function in the Poisson equation (12) the dispersion equation for the twisted plasma wave is obtained:

$$\epsilon(\omega, k) = 1 + \frac{e^2}{\epsilon_0 k^2}\int d\mathbf{v}\left[-1 + \frac{\omega(\omega - kv_z)}{(\omega - kv_z)^2 + Q^{(l)}_{p,p}v_\perp^2/w_b^2}\right] \times \partial_\varepsilon f_{e0} = 0. \quad (24)$$

The solution of this equation in the limit $\omega \gg kv_{\rm th}$, where $v_{\rm th}$ is the electron thermal velocity, can be found by using a standard expansion procedure. Here we consider the equilibrium distribution function (8), but the expression (24) is more general. A nonequilibrium distribution function may result from the corresponding plasma wave modes. The real part of the dispersion equation (24) then reads

$$\mathrm{Re}[\epsilon(\omega, k)] = 1 - \frac{\omega_{pe}^2}{\omega^2}\left(1 + \frac{3k^2v_{\rm th}^2}{\omega^2} - \frac{2Q^{(l)}_{p,p}}{k^2w_b^2}\right),$$

where $\omega_{pe} = \sqrt{e^2n_{e0}/m_e\epsilon_0}$ is the plasma frequency. The mode-coupling term contributes then to the plasma wave dispersion:

$$\omega^2 = \omega_{pe}^2\left(1 + 3k^2\lambda_{\rm De}^2 - 2Q^{(l)}_{p,p}/k^2w_b^2\right). \quad (25)$$

Here $\lambda_{\rm De} = v_{\rm th}/\omega_{pe}$ is the Debye length. The last term in the parenthesis could be comparable with the thermal dispersion. As it is shown below in Eq. (29) the coefficients $Q^{(l)}_{p,p}$ are negative and consequently the OAM and final radial extension of the plasma wave increase its dispersion.

By taking the residue in the resonance terms in the right-hand side of Eq. (24) one finds an expression for the plasma wave damping. The Landau resonance in the case of plane wave $v_z = \omega/k$ splits into two resonances $v_z^{\pm} = \omega/k \pm (v_\perp/kw_b)\sqrt{-Q^{(l)}_{p,p}}$ shifted with respect to the axial phase velocity. By considering the residues of these two resonances one finds expression for the imaginary part of the dielectric permittivity:

$$\mathrm{Im}[\epsilon(\omega, k)] = \sqrt{\frac{\pi}{2}}\frac{\omega_{pe}^2\omega}{k^3v_{\rm th}^3}\exp\left(-\frac{\omega^2}{2k^2v_{\rm th}^2}\right) \times R\left(\frac{2\omega}{k^2v_{\rm th}w_b}\sqrt{-Q^{(l)}_{p,p}}\right). \quad (26)$$

Here, the function $R(\xi) = \int_0^\infty du\, u\, \exp(-u^2/2)\cosh(u\xi)$ accounts for the OAM contribution. The corrections due to the orbital momentum of the plasma wave are of the same order to the dispersion and to the damping. The quantitative contribution is defined by the value of the coupling coefficient $Q^{(l)}_{p,p}$.

Calculation of the coefficients $K^{\pm}$ is presented in Appendix A. There are only four nonzero terms in the coefficients K^{-}:

$$K^{-}_{p,l;p,l-1} = -\frac{1}{2}\left(1 - i\frac{z}{z_R}\right)\sqrt{l+p},$$
$$K^{-}_{p,l;p+1,l-1} = -\frac{1}{2}\left(1 + i\frac{z}{z_R}\right)\sqrt{p+1},$$
$$K^{-}_{p-1,l+1;p,l} = -\frac{1}{2}\left(1 + i\frac{z}{z_R}\right)\sqrt{p},$$
$$K^{-}_{p,l+1;p,l} = -\frac{1}{2}\left(1 - i\frac{z}{z_R}\right)\sqrt{l+p+1}. \quad (27)$$

The corresponding matching coefficients in the series K^{+} read

$$K^{+}_{p,l-1;p,l} = \frac{1}{2}\left(1 + i\frac{z}{z_R}\right)\sqrt{l+p},$$
$$K^{+}_{p+1,l-1;p,l} = \frac{1}{2}\left(1 - i\frac{z}{z_R}\right)\sqrt{p+1},$$
$$K^{+}_{p,l;p-1,l+1} = \frac{1}{2}\left(1 - i\frac{z}{z_R}\right)\sqrt{p},$$
$$K^{+}_{p,l;p,l+1} = \frac{1}{2}\left(1 + i\frac{z}{z_R}\right)\sqrt{l+p+1}. \quad (28)$$

Summing these coefficients according to Eq. (22) one finds the final expression for the coupling coefficient:

$$Q^{(l)}_{p,p'} = -\left(1+\frac{z^2}{z_R^2}\right)\left(p+\frac{|l|+1}{2}\right). \tag{29}$$

As one can see, the mode p, l is coupled in general to four neighboring modes: $p, l\pm1$ and $p\pm1, l\mp1$. In the case $p=0$ only three modes are coupled: 0, $l\pm1$ and 1, $l-1$. Finally, the principal mode 0,0 is coupled to two modes 0,1 and 1, -1.

All coupling coefficients are negative. This implies, in agreement with qualitative expectations, that presence of OAM increases the plasma wave dispersion and damping. The final expressions can be written as follows:

$$\omega^2 = \omega_{pe}^2\left(1+3k^2\lambda_{\rm De}^2+\frac{2p+|l|+1}{k^2w_b^2}\right), \tag{30}$$

$$\frac{{\rm Im}\,\omega}{\omega} = -\sqrt{\frac{\pi}{8}}\frac{1}{k^3\lambda_{\rm De}^3}\exp\left(-\frac{\omega^2}{2k^2v_{\rm th}^2}\right) \times R\left(\frac{\sqrt{p+(|l|+1)/2}}{k^2\lambda_{\rm De}w_b}\right). \tag{31}$$

Note that these expressions are rather different from the expressions (26) and (30) for the plasma wave dispersion and damping proposed in Ref. [8]. In the limit of a very wide (almost planar) wave one finds the standard expressions for the dispersion and damping of a plane Langmuir wave. In contrast, in the case of sufficiently narrow beams, where $kw_{b,0} < 1/k\lambda_{\rm De}$, the OAM corrections dominate, the function R in that limit $\xi \gg 1$ behaves as $R(\xi)\sim\sqrt{2\pi}\,\xi\,\exp(\xi^2/2)$. Graphical representations of these two functions with comparisons to the standard dispersion relation and damping are presented in Fig. 1. As expected, we observe that the OAM carried by plasma waves impacts dispersion and damping terms as the plasma wave narrows, resulting in an increase of both terms.

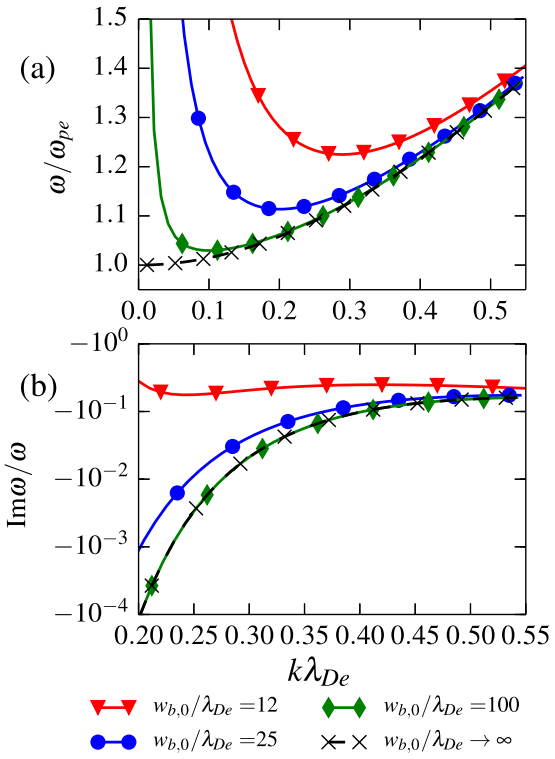

FIG. 1. Dispersion (a) and damping (b) of the OAM plasma wave calculated using Eqs. (30) and (31). Values on these graphs are calculated using the wave width $w_{b,0}/\lambda_D = 12$ (red triangles), 25 (blue circles), and 100 (green diamonds) and for the OAM conditions $l=2$, $p=0$. The black crossed line on (a) shows the standard Bohm-Gross dispersion corresponding to $w_{b,0}/\lambda_D\to\infty$, while the black dashed line on (b) shows the damping rate in the limit $k^2\lambda_{\rm De}w_{b,0}\gg1$.

III. STRUCTURE OF A VORTICAL PLASMA WAVE

A. Electric field of a plasma wave carrying an orbital momentum

As an example of LG plasma wave con sidered in the previous section, we consider here a structure of a single mode p, l within the Rayleigh zone $|z|\ll z_R$. The electric potential (9) contains only one term characterized by the amplitude $\phi_{p,l}$:

$$\Phi(z,r,\theta) = \phi_{p,l}F_{p,l}(X)\,\cos(kz-\omega t+l\theta), \tag{32}$$

where the radial part is given by the function $F_{p,l}(r^2/w_b^2)$ (4). The electric field is found by taking the gradient of the potential:

$$E_z = E_0F_{p,l}(X)\,\sin(kz-\omega t+l\theta), \tag{33}$$

$$E_\theta = \frac{lE_0}{kw_b}X^{-1/2}F_{p,l}(X)\,\sin(kz-\omega t+l\theta), \tag{34}$$

$$E_r = -2\frac{E_0}{kw_b}X^{1/2}F'_{p,l}(X)\,\cos(kz-\omega t+l\theta), \tag{35}$$

where $E_0 = k\phi_{p,l}$ is the amplitude of the axial electric field. The axial field dominates; the transverse fields are smaller by a factor $1/kw_b\ll1$. The radial field is phase shifted with respect to the azimuthal and axial fields.

It is important to assure that the radial and azimuthal electric fields are not singular at the beam axis. As the radial function behaves at the origin $X\ll1$ as $F_{p,l}\propto X^{|l|/2}$, the fields in question behave as $E_\theta\propto r^{|l|-1}$ and $E_r\propto r^{|l|-1}$. Therefore, for $l=\pm1$ these fields are nonzero at the axis,

$$E_\theta(r=0) = \pm\frac{E_0}{kw_{b,0}}\sqrt{p+1}\,\sin(kz-\omega t\pm\theta),$$

$$E_r(r=0) = -\frac{E_0}{kw_{b,0}}\sqrt{p+1}\,\cos(kz-\omega t\pm\theta).$$

This mode $l=1$ has been excited in Ref. [6]. We can better understand the structure of the mode $l=\pm1$ by presenting these fields in the Cartesian coordinates:

$$E_x(x=0,y=0) = -\frac{E_0}{kw_{b,0}}\sqrt{p+1}\,\cos(kz-\omega t),$$

$$E_y(x=0,y=0) = \pm\frac{E_0}{kw_{b,0}}\sqrt{p+1}\,\sin(kz-\omega t).$$

These fields are regular; they correspond to the field of a dipole rotating in the clockwise direction.

B. Electron distribution function in the field of a plasma wave

The dominant term in the expansion of the electron distribution function (10) is given by Eq. (23). In the first-order expansion over the paraxial parameter $1/kw_b \ll 1$, the expression is straightforward:

$$f_{p,l}^{(0)} = \frac{kv_z}{\omega - kv_z} e\phi_{p,l}\partial_\varepsilon f_{e0}. \tag{36}$$

However, there are other coefficients that are of the first order. This follows from Eq. (20) by taking into account the fact that nonzero coefficients are given by Eqs. (27) and (28). The three components of the electron distribution function in the first order are the following:

$$f_{p,l\pm1}^{(\pm1)} = \pm\frac{iv_\perp}{2w}\frac{\omega}{(\omega - kv_z)^2} e\phi_{0,1}\partial_\varepsilon f_{e0}\sqrt{l + p + \frac{1 \pm 1}{2}}, \tag{37}$$

$$f_{p\mp1,l\pm1}^{(\pm1)} = -\frac{iv_\perp}{2w}\frac{\omega}{(\omega - kv_z)^2} e\phi_{0,1}\partial_\varepsilon f_{e0}\sqrt{p + \frac{1 \mp 1}{2}}. \tag{38}$$

With these expressions one can calculate the explicit form of the electron distribution function:

$$\begin{aligned}\delta f_e = \frac{eE_0}{\omega - kv_z}\partial_\varepsilon f_{e0}\Bigg[& v_z F_{p,l}(X)\cos(kz - \omega t + l\theta) \\ & + \frac{v_\theta l}{kw_b}\frac{\omega}{\omega - kv_z} X^{-1/2} F_{p,l}(X)\cos(kz - \omega t + l\theta) \\ & - 2\frac{v_r}{kw_b}\frac{\omega}{\omega - kv_z} X^{1/2} F'_{p,l}(X)\sin(kz - \omega t + l\theta)\Bigg].\end{aligned} \tag{39}$$

Here the radial and azimuthal electron velocities $v_r = v_\perp\cos(\theta - \theta_v)$ and $v_\theta = -v_\perp\sin(\theta - \theta_v)$ are introduced the same way as in Eqs. (16) and (17). Coupling of the dominant mode p, l to neighboring modes results in the appearance of azimuthal and radial electron velocities in the expression for the electron distribution function.

This expression can be used for the calculation of the moments of electron distribution function. The lowest moments, the perturbation of density and electric current, can also be found directly from the Poisson and Ampere equations. Explicit solutions for the electron distribution function for mode $p = 0$, $l = 2$ are derived in Appendix B. According to Eq. (7), the density perturbation reads

$$\frac{\delta n_e}{n_{e0}} = -\frac{keE_0}{m_e\omega_{pe}^2} F_{p,l}(X)\cos(kz - \omega t + l\theta). \tag{40}$$

The electric current follows from the Ampere relation, $\mathbf{j}_e = -\epsilon_0\partial_t\mathbf{E}$:

$$j_z = \epsilon_0\omega E_0 F_{p,l}(X)\cos(kz - \omega t + l\theta), \tag{41}$$

$$j_\theta = \epsilon_0\omega\frac{lE_0}{kw_b} X^{-1/2} F_{p,l}(X)\cos(kz - \omega t + l\theta), \tag{42}$$

$$j_r = 2\epsilon_0\omega\frac{E_0}{kw_b} X^{1/2} F'_{p,l}(X)\sin(kz - \omega t + l\theta). \tag{43}$$

The same expressions can be found by integrating the expression (39) for the electron distribution function and accounting for the dispersion relation $\omega \approx \omega_{pe}$. One can also calculate the orbital momentum carried by electrons in the plasma wave. In the first order on the wave amplitude one finds

$$\begin{aligned} l_z &= m_e r\int d\mathbf{v}\, v_\theta \delta f_e \\ &= -\frac{n_{e0}}{\omega} eE_0 X^{-1/2} F_{p,l}(X)\cos(kz - \omega t + l\theta). \end{aligned} \tag{44}$$

It oscillates in space and time and does not create a magnetic field.

C. Numerical modeling

In order to test the analytical results presented in this article we carry out numerical calculations in a kinetic framework. These numerical calculations are performed using the particle-in-cell (PIC) code OCEAN [11]. A three-dimensional (3D) box with dimensions $1200 \times 1200 \times 160$ cubic cells with sides of length $\delta l = \lambda_{\mathrm{De}}$ is filled with a uniform hydrogen plasma to a density $n_{e,0}$ and temperature of $T_e/m_e c^2 = 1.54 \times 10^{-3}$, while ions are fixed. In order to properly resolve fields at nonrelativistic amplitudes more than 100 particles per cell are required to achieve a high enough signal-to-noise ratio to measure second-order effects. The boundary condition along the propagation axis is periodic, while in the transverse directions they are absorbing for both fields and particles. In order to facilitate a simple periodic plasma wave with OAM the Gouy phase and front curvature are ignored for this analysis.

Simulations model a plasma wave with an OAM mode of $p = 0$, $l = 2$, and assuming a phase velocity $\omega/k = c$ to avoid damping and trapped particles. The length of the box was chosen so that it fits exactly one wavelength with $kL_z = 2\pi$. The width of the plasma wave $w_b/\lambda_{\mathrm{De}} = 400/\pi$ being chosen so that $kw_b \gg 1$ to reduce additional dispersion from the vortex terms in Eq. (30) and so that $k^2 w_b\lambda_{\mathrm{De}} \gg 1$ to reduce the vortex terms in Eq. (31).

No electromagnetic field is considered to excite the plasmon. To model this wave we impose a perturbative electric field of the form described in Eqs. (33)–(35). This perturbation is imposed volumetrically on each time step with the dimensionless amplitude $\delta a_0 = eE_0/m_e c\omega_{pe}N_{dt}$, where N_{dt} is a number of time steps over 10 plasma periods so that $N_{dt} = 10T_{pe}/dt$. The value of δa_0 is chosen so that the resulting perturbation increases linearly from zero to the maximum value $a_0 = 0.3$. After that time the wave is allowed to evolve freely in plasma without any driver over more than 20 periods. Such a method of plasma wave excitation is not 100% efficient and it results in the maximum amplitude of the free plasma wave of $a_0 = 0.2$. That difference between the imposed and observed field of the plasma wave is explained by an impedance to the system due to the thermal effects and the positioning of the absorbing boundaries.

Figure 2 compares the simulation results for electron density, azimuthal, and radial electric fields with theoretical values given by Eqs. (40), (34), and (35) with $a_0 = 0.2$. The transverse slices given in the left column clearly display four azimuthal lobes expected for an $l = 2$ mode; the more detailed comparison on the right shows line outs from the numerical calculations comparing extremely well with the theoretical mode. The line-out plots shown in the figure are filtered using a Gaussian filter with a width of one cell, which removes the high-frequency noise; the results without the filter are also

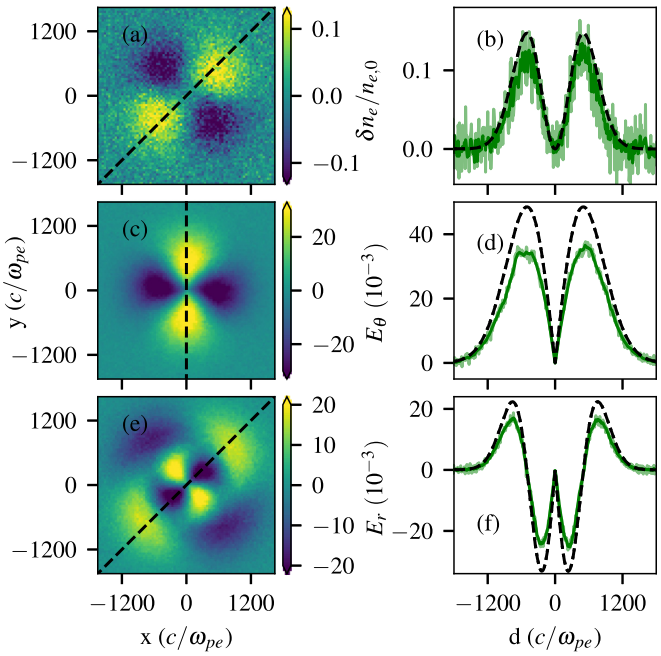

FIG. 2. Results from a PIC simulation 16 periods after the initial 10-period setup phase. The plots on the top are of $\delta n_e/n_{e0}$, the middle of E_θ, and the bottom of E_r. The electric fields are normalized by the plasma field $E_p = m_e c\omega_{pe}/e$. The plots on the left, (a), (c), and (e), show transverse slices (with no image filter applied) taken from the center of the PIC code box, with the propagation (z) axis going into the page. The dashed lines shown in the transverse slices are the line outs used to plot the graphics on the right. The plots on the right, (b), (d), and (f), are line outs from the slices (filtered green, unfiltered light green) compared with theoretical predictions with an $a_0 = 0.2$ (black dashed lines) plotted against the position along the line outs d plotted in (a), (c), and (e); this corresponds to $y\cos\phi$ where ϕ is the angle the line out would make with the y axis.

shown for comparison. More details of the setup and stability of the simulation are described in Appendix C.

D. Magnetic field generation in the field of a plasma wave

Equation (44) shows that no magnetic field is generated in the first order. However, it was shown in Ref. [12] that a magnetic field can be generated as a result of second-order effects. The general expressions for the magnetic field generation by a plasma wave are derived by Bell *et al.* [12] and Gorbunov *et al.* [13]. Following the approach developed in this paper, the equation for the second-order vector potential $\mathbf{A}^{(2)}$ can be written as

$$\left(\partial_t^2 - c^2\nabla^2 + \omega_{pe}^2\right)\mathbf{A}^{(2)} = \epsilon_0^{-1}\mathbf{j}^{(2)}, \tag{45}$$

where $\mathbf{j}^{(2)} = -e\delta n_e \mathbf{v}_e = \mathbf{j}\,\delta n_e/n_{e0}$ is the second-order current. According to the expressions (40)–(43), all three components of the vector potential are generated in the second order on the plasma wave amplitude. Explicit expressions for the vector potential can be found from Eq. (45) in the paraxial approximation, accounting only for the dominant axial derivative in the Laplacian term:

$$A_z = -\frac{ekE_0^2}{2m_e\omega^3}F_{p,l}^2 - \frac{ekE_0^2}{2m_e\omega}\frac{F_{p,l}^2}{4k^2c^2 - 3\omega^2} \times \cos 2(kz - \omega t + l\theta), \tag{46}$$

$$A_\theta = -\frac{elE_0^2}{2m_e\omega^3 w_b}X^{-1/2}F_{p,l}^2 - \frac{elE_0^2}{2m_e\omega w_b}\frac{X^{-1/2}F_{p,l}^2}{4k^2c^2 - 3\omega^2}\cos 2(kz - \omega t + l\theta), \tag{47}$$

$$A_r = -\frac{eE_0^2}{2m_e\omega w_b}\frac{X^{1/2}(F_{p,l}^2)'}{4k^2c^2 - 3\omega^2}\sin 2(kz - \omega t + l\theta). \tag{48}$$

It contains quasistationary components for the axial and azimuthal components and the component oscillating at the second harmonic. The axial component dominates and two other components are of the first order on the paraxial parameter. The magnetic field $\mathbf{B} = \nabla \times \mathbf{A}^{(2)}$ calculation is straightforward:

$$B_z = -\frac{elE_0^2}{m_e\omega^3 w_b^2}\left(F_{p,l}^2\right)', \tag{49}$$

$$B_\theta = \frac{ekE_0^2}{m_e\omega^3 w_b}X^{1/2}\left(F_{p,l}^2\right)'. \tag{50}$$

The radial component of the magnetic field is zero, $B_r = 0$, with the relationship between the azimuthal and axial components being $B_\theta/B_z = (kw_b/l)X^{1/2}$. It is of the first order on the paraxial parameter compared to the axial component which is of the second order. The magnetic field is constant; it does not oscillate in time and in space. Magnetic field lines form helices of a constant radius rotating in the direction opposite to the sign of the orbital momentum: $\theta = \theta_0 - (k/l)(z - z_0)$. An illustration of such a magnetic field is presented in Fig. 3 for the mode $p = 0$, $l = 2$ where several 3D representations of the data from the numerical simulation are given. The red and blue surfaces show isodensity contours for positive and negative perturbations; we note the four azimuthal lobes of the $l = 2$ mode. The green and purple lines display the interior and exterior magnetic field lines, which do not oscillate in time.

It is important to note that the total magnetic flux over any closed surface is zero: $\oint \mathbf{B}\cdot d\mathbf{S} = \int dV\,\nabla\cdot\mathbf{B} = 0$. In particular, $\int_0^\infty B_z r\,dr = 0$ and magnetic field is zero at the axis. Generation of that magnetic field is an adiabatic effect. Its intensity is proportional to the square of the plasma wave electric field and it disappears as soon as the plasma wave disappears.

The azimuthal component of magnetic field is created by the quasistatic electric current associated with the axial momentum carried with the plasma wave. The axial component of the magnetic field can be related to the orbital momentum carried by the plasma wave. The latter can be derived from the general expression for the electromagnetic stress tensor [14]. In the case of a zero magnetic field it reads $T_{ij} = \epsilon_0(E_iE_j - \frac{1}{2}\delta_{ij}E^2)$. In plasma we need also to add the particle stress tensor $\sigma_{ij} = n_{e0}m_e u_i u_j$. Then the wave

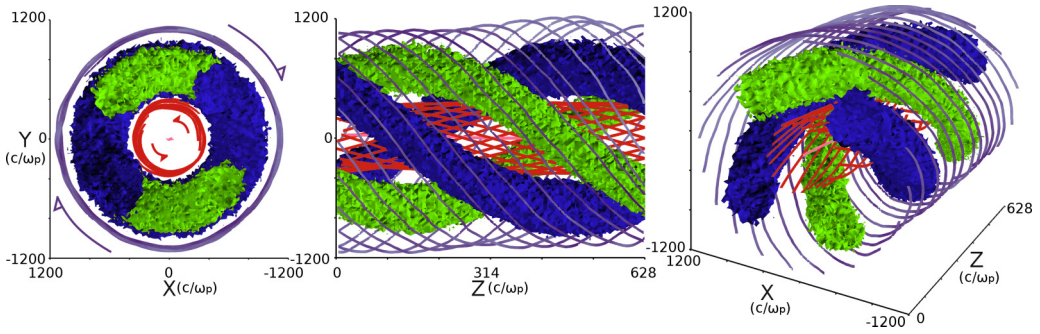

FIG. 3. Three 3D views of the electron density deviation in the plasma wave, calculated in the OCEAN PIC code for the plasmon mode $p = 0$, $l = 2$, data taken 16 periods after the initial 10 period setup phase. The views along the propagation axis, and across the transverse axis, are shown with a parallel projection, and the final tilted image uses a convergent projection. The red and blue surfaces show surfaces of constant $\delta n_e/n_{e0}$, and the light green surface corresponds to a positive density perturbation with a value of 80% the amplitude of the plasmon. The dark blue surface shows a negative density perturbation with the same absolute value as the red surface. In addition to the surfaces of constant density the magnetic field lines for the interior (interior red thin lines) and exterior (exterior light thin purple lines) regions of the plasmon are shown. The magnetic field lines are calculated using the magnetic field values taken from the PIC code and the MAYAVI2 [15] streamline package; the first figure includes arrows to denote the direction of propagation of the magnetic field lines.

momentum is described by the projection of the stress tensor on the correspondent direction divided by the phase velocity, $P_j = (k/\omega)\sum_j n_i(T_{ij} + \sigma_{ij})$. The dominant term in the expression for the axial component of the orbital momentum reads

$$L_z = rP_\theta k/\omega = r\,(k/\omega)\,(\epsilon_0 E_z E_\theta + n_{e0} m_e u_z u_\theta) = \frac{\epsilon_0 l}{\omega} E_0^2 F_{p,l}^2. \tag{51}$$

Correspondingly, the total orbital momentum per unit length carried with a twisted plasma wave is $\mathcal{L}_z = 2\pi \int_0^\infty r\,dr L_z = \pi w_b^2 \epsilon_0 l E_0^2/\omega$. [Here the relation (6) for the normalization of the radial functions is used.] One then can define the magnetic moment per unit volume,

$$M_z = -\frac{e}{m_e} L_z = -\frac{\epsilon_0 e l}{m_e \omega} E_0^2 F_{p,l}^2,$$

and the total magnetic moment per unit length $\mathcal{M}_z = -\pi w_b^2 \epsilon_0 e l E_{0,1}^2/m_e\omega$. It can be noticed that one cannot obtain the same expression for the magnetic moment by applying the definition of the magnetic moment of electrons as $M_z = r j_\theta^{(2)} = r j_\theta \delta n_e/n_{e0}$. The component of magnetic moment carried with the plasma wave field is lost in such a definition.

The magnetic fields at later times in the PIC code (Fig. 4) show a twisted solenoidlike magnetic field which matches the theoretical calculation above. The numerical values of the magnetic field match theoretical calculations even after the plasmon is left to oscillate for ∼20 periods, despite being close to the noise threshold of the PIC calculation.

The plasmon described in Ref. [9] appears to have the same form and the same amplitude as that described in this paper. With a plasmon of amplitude $a_0 = 0.15 - 0.25$, an OAM mode $p = 0$, $l = 2$, a plasma density $n_{e0} = 4.5 \times 10^{18}$ cm^{-3}, and a beam waist $w_{b,0} = 5\,\mu$m the peak value in the axial direction is 2.5–6.9 T, which is consistent with magnetic field plotted in Fig. 2 of Ref. [9]. The azimuthal field in this case, assuming a value of $k = \omega_{pe}/c$ from the wave matching conditions used in said paper, would have a similar peak value to the axial components at 2.0–5.8 T. The theoretical analysis undertaken in Ref. [9] involves considering ringlike current structure that ignores the axial components, however, this would not be sufficient to calculate the azimuthal magnetic field. No azimuthal magnetic field is shown in the numerical results, and so the full structure of the magnetic field cannot be commented on further.

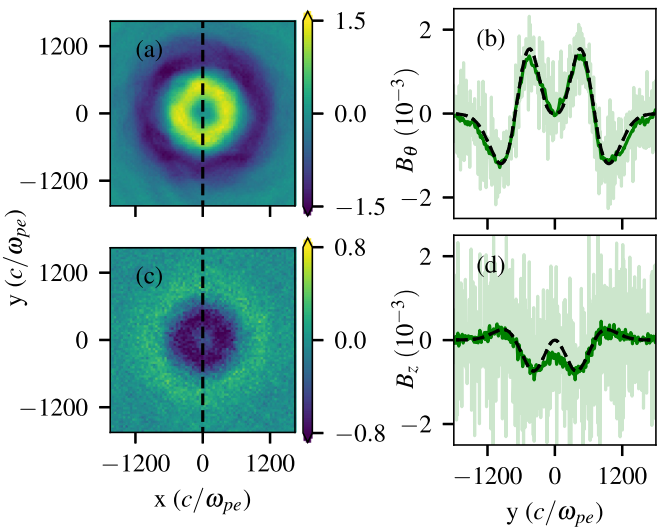

FIG. 4. Results from the same PIC simulation as in Fig. 2. The plots on the top show the azimuthal magnetic field B_θ and the bottom show the axial magnetic field B_z, both normalized to the field $B_p = m_e\omega_{pe}/e$. The plots on the left show the central transverse slice from the PIC box (filtered using a Gaussian filter with a width equal to one cell and the plots on the right show line outs from these slices (light green unfiltered data, green filtered data) compared with a theoretical model using $a_0 = 0.2$ (black dashed line). Due to this being a second-order effect there is considerable noise seen in the magnetic field, despite there being ∼100 particles per cell in the simulation. Nevertheless, after a filter is applied to the axial field, a good match to the theoretical model can be seen.

IV. CONCLUSIONS

This study of electrostatic electron plasma waves with orbital angular momentum covers two main aspects of the physics of these objects. The first aspect being the development of a fully kinetic paraxial perturbation applied to the electron distribution function. The analysis presented here includes corrections due to the coupling of nearest-neighbor modes due to gradient terms in the linearized Vlasov equation. This new electron distribution function is used to develop a dispersion equation allowing for the calculation of the phase and group velocities of such a plasma wave including this coupling. The wave orbital momentum and final radial extent result in a stronger wave dispersion and stronger damping. These effects become particularly important for the plasma waves with wavelengths larger than $kw_{b,0}\lambda_{\mathrm{De}}$. It is expected that the collisionless damping of the twisted plasma wave will result in the transfer of the wave orbital momentum to the resonant electrons. The analytical results shown in this study can be extended to higher amplitudes, if nonlinear phenomena and wave breaking of plasma waves with the additional OAM components will be considered.

The second subject of this study is magnetic field generation by an OAM plasmon. While the first-order field is shown to be zero, in the second order a significant "twisted solenoidlike" magnetic field is shown to exist in both theoretical calculations and particle-in-cell simulations.

ACKNOWLEDGMENTS

This work was granted access to HPC resources of TGCC under the allocation A0010506129 made by GENCI. We acknowledge PRACE for awarding us access to resource Joliot Curie-SKL based in France at TGCC Center. The authors acknowledge support from MEPhI Academic Excellence Project (Contract No. 02.a03.21.0005-27.08.2013) and from the project ELITAS (ELI Tools for Advanced Simulation) CZ.02.1.01/0.0/0.0/16_013/0001793 from the European Regional Development Fund.

APPENDIX A: CALCULATION OF THE COUPLING COEFFICIENTS

Expression (14) for the derivative of $F_{p,l}$ can be obtained by using expression (5) for the Laguerre polynomial. By taking a derivative of this expression one finds $x(L_p^l)' = (p+1)L_{p+1}^{l-1} - (l-x)L_p^l$. At the same time, the Laguerre polynomial can also be expressed in a power series [10]:

$$L_p^l(x) = \sum_{k=0}^{p}(-1)^k \frac{(p+l)!\,x^k}{k!\,(p-k)!\,(l+k)!}. \tag{A1}$$

By taking the derivative of this expression one finds another presentation: $(L_p^l)' = -L_{p-1}^{l+1}$. Combining both expressions for the derivatives one has a relation between the Laguerre polynomials of different order:

$$xL_{p-1}^{l+1}(x) = -(p+1)L_{p+1}^{l-1} + (l-x)L_p^l. \tag{A2}$$

This expression allows the presentation of the derivative of $F_{p,l}$ in the form given by Eq. (14).

The mode-coupling coefficient is given by Eq. (22). The coefficients entering in this expression contain integrals of a product of two Laguerre polynomials multiplied by a power and exponential function:

$$I_j(p,l;p',l') = \int_0^\infty dx\, x^j e^{-x} L_p^l(x) L_{p'}^{l'}(x). \tag{A3}$$

The method of evaluation of that integral consists in two steps. First, the Laguerre polynomial with an index p' is developed in a power series according to Eq. (A1):

$$I_j(p,l;p',l') = \sum_{k=0}^{p'}(-1)^k \frac{(p'+l')!}{k!\,(p'-k)!\,(l'+k)!} \times \int_0^\infty dx\, x^{j+k} e^{-x} L_p^l(x). \tag{A4}$$

The remaining integral can be calculated as follows: In the case $0 \leqslant j+k \leqslant l-1$ its value is given in Ref. [10], Eq. (7.414.11):

$$\int_0^\infty dx\, e^{-x} x^{j+k} L_p^l(x) = \frac{(j+k)!\,(l+p-j-k-1)!}{p!\,(l-j-k-1)!}.$$

In the case $j+k \geqslant l$ the remaining Laguerre polynomial L_p^l can be represented according to Eq. (5):

$$\int_0^\infty dx\, e^{-x} x^{j+k} L_p^l(x) = \frac{1}{p!}\int_0^\infty dx\, x^{j+k-l} d_x^p\left(e^{-x}x^{l+p}\right).$$

The integral in the right-hand side is calculated by integrating it by parts p times. It has nonzero value only if $j+k \geqslant l+p$:

$$\int_0^\infty dx\, \mathrm{e}^{-x} x^{j+k} L_p^l(x) = (-1)^p \frac{(j+k)!\,(j+k-l)!}{p!\,(j+k-l-p)!}.$$

Inserting these expressions in Eq. (A4) we find a representation for the integral $I_j(p,l;p',l')$ as a finite sum:

$$I_j(p,l;p',l') = \sum_{k=0}^{p'}(-1)^k \frac{(p'+l')!\,(j+k)!}{p!\,k!\,(p'-k)!\,(l'+k)!} \begin{cases} \frac{(p+l-j-k-1)!}{(l-j-k-1)!}, & k \leqslant l-j-1, \\ 0, & l-j \leqslant k \leqslant p+l-j-1, \\ (-1)^p \frac{(j+k-l)!}{(j+k-p-l)!}, & k \geqslant p+l-j. \end{cases} \tag{A5}$$

By using that expression for $I_j(p,l;p',l')$ one can calculate explicitly the expressions for the coefficients $K^{\pm}$. Because of the symmetry $I_j(p,l,p',l') = I_j(p',l',p,l)$, the summation limits $p+l-j \leqslant p'$ and $p'+l-j \leqslant p$ need $p'+l-j \geqslant$

$p \geqslant p' - l + j$ and $l + l' \leqslant 2j$. Then the nonzero coefficients needed for calculation of the coupling coefficient Q_{pp} are given by Eqs. (27) and (28).

APPENDIX B: ELECTRON DISTRIBUTION FUNCTION OF THE VORTICAL MODE (0, 2)

Here we present an example of the electron distribution function for an LG plasma wave, considered in Sec. III, of the mode $p = 0$, $l = 2$, and for simplification the Gouy phase and front curvature are ignored. The corresponding radial functions read

$$F_{0,2} = X/\sqrt{2}\, e^{-X/2}, \quad F_{1,1} = \sqrt{X/2}\,(2 - X)\, e^{-X/2}.$$

The electric potential (9) contains only one term characterized by the amplitude $\phi_{0,2}$:

$$\Phi = \frac{\phi_{0,2}}{\sqrt{2}} \frac{r^2}{w_b^2} e^{-r^2/2w_b^2} \cos(kz - \omega t + 2\theta).$$

The electric field can then be found by taking the gradient of the potential. The dominant term in the expansion of the electron distribution function (10) is given by Eq. (23). In the first-order expansion over the paraxial parameter $1/kw_b \ll 1$, the expression is straightforward:

$$f_{0,2} = \frac{kv_z}{\omega - kv_z} e\phi_{0,2} \partial_\varepsilon f_{e0}.$$

Other coefficients are of the first order. They are following from Eq. (20) by taking into account the fact that nonzero coefficients are given by Eqs. (27) and (28). The three components of the electron distribution function in the first order are the following:

$$f_{0,2\pm1} = \frac{iv_\perp}{2w} \frac{\omega}{(\omega - kv_z)^2} e\phi_{0,2} \partial_\varepsilon f_{e0}\, e^{\mp i\theta_v} \sqrt{2 + \frac{1 \pm 1}{2}},$$

$$f_{1,0} = -\frac{iv_\perp}{2w} \frac{\omega}{(\omega - kv_z)^2} e\phi_{0,2} \partial_\varepsilon f_{e0}\, e^{i\theta_v}.$$

With these expressions one can calculate the explicit form of the electron distribution function:

$$\frac{\delta f_e}{f_{e0}} = -\frac{a_0 c}{\sqrt{2} v_{\rm th}^2} \frac{\omega}{\omega - kv_z} \frac{r}{w_b} e^{-r^2/2w_b^2} \left[v_z \frac{r}{w_b} \cos(kz - \omega t + 2\theta) + \frac{v_\theta}{kw_b} \frac{\omega}{\omega - kv_z} \cos(kz - \omega t + 2\theta) + \frac{v_r}{kw_b} \frac{\omega}{\omega - kv_z} \left(\frac{r^2}{w_b^2} - 2 \right) \sin(kz - \omega t + 2\theta) \right].$$

Here the dimensionless amplitude $a_0 = ek\phi_{0,2}/m_e\omega c$ is introduced. This expression can be used for calculation of the moments of the electron distribution function.

APPENDIX C: NUMERICAL MODELING TECHNIQUES

There are several ways that a plasma oscillation can be independently generated in a PIC simulation: by imposing a perturbation on the electron distribution function and solving the Gauss equation for a potential, or by imposing an electric field of the correct form to generate the electron distribution function associated with the desired plasmon. The latter method has the advantage that it can be performed gradually in time. Since one of the principle aims of the simulation presented here is to demonstrate the existence of certain second-order effects, a gradual onset method, as described in Sec. III C, gives the system time to relax into a stable state.

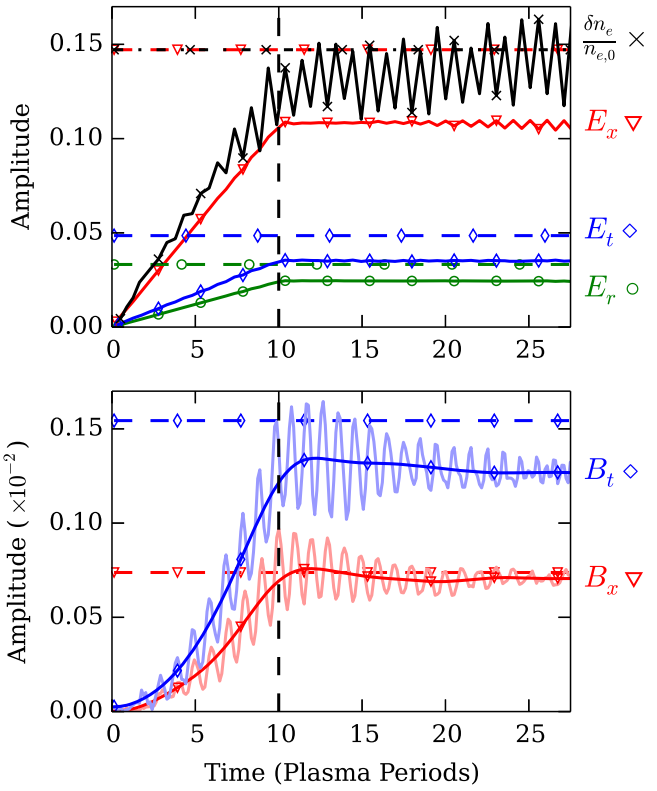

FIG. 5. The upper plot shows the amplitude of the electric field components, with red triangles showing the axial, blue diamonds the azimuthal, green circles the radial electric fields, and finally black crosses showing the electron density component. The vertical dashed line shows the point in the simulation where the amplification process stops. The horizontal dashed lines show the component amplitudes for a reference $a_0 = 0.2$ in the same color and marker scheme. The lower plot shows the amplitude of magnetic field components in the PIC simulation. Red lines with triangles correspond to the axial field, and blue lines with diamonds to the azimuthal field, with the solid line corresponding to the PIC simulation; the darker solid line corresponds to an average over a Gaussian window over three periods. No radial magnetic field is observable.

The plasmon generated in the simulation presented here attains an amplitude in the range $0.1 < a_0 < 0.2$. The electric field across all components achieved a consistent amplitude of $a_0 = 0.15 \pm 0.01$. The electron density component of the plasmon has some nonlinear features where the positive density part of the wave has a slightly larger amplitude than the negative density part; both the negative and positive amplitudes correspond to an a_0 in the range $0.2 > a_0 > 0.15$. Dependence of the amplitudes of the electric and magnetic fields on time can be seen in Fig. 5. They are normalized to $m_e c\omega_{pe}/e$ and $m_e\omega_{pe}/e$, respectively. The frequency of the plasmon matches that described by the dispersion relation Eq. (A4), which in this case reduces to the simple result $\omega \simeq \omega_{pe}$, with all electric field and density components oscillating

with the same frequency. The single plasmon observable in the simulation is stable for the duration of the simulation (∼20 oscillations) after the initial 10 oscillation setup phase.

To run a simulation with a grid consisting of $1200 \times 1200 \times 160$ cells and 100 particles per cell, approximately 24 h on 20 000 cores is required. Such a high resolution is required for several reasons: the first reason being that the temperature is required to be low to avoid such effects as wave breaking and Landau damping; the second reason being that when a lower resolution is used the amplification process is less efficient as the observed plasmon becomes out of phase with the amplifying field; thirdly the second-order magnetic fields are not observable in conditions with greater noise. If the grid size is reduced by a factor of 4 and the number of particles reduced to just 10 per cell a stable plasma wave of the same amplitude is still observable for the duration of the simulation.

The amplitude of the two components of the magnetic field correspond to an a_0 in the range $0.2 > a_0 > 0.15$ consistent with the amplitude observed in the electron density component. The profile of the magnetic field, while static in space, has some temporal oscillation (see Fig. 5) at a frequency of ω_{pe} during the amplification phase but with a small amplitude of around 10%–20% of the mean value and decaying in time towards an equilibrium value. At very late in time an oscillation at a frequency of $2\omega_{pe}$ is visible in the azimuthal field.

[1] L. Allen, M. W. Beijersbergen, R. J. C. Spreeuw, and J. P. Woerdman, Orbital angular momentum of light and the transformation of Laguerre-Gaussian laser modes, Phys. Rev. A **45**, 8185 (1992).

[2] Q. Zhan, Cylindrical vector beams: From mathematical concepts to applications, Adv. Opt. Photonics **1**, 1 (2009).

[3] J. Vieira and J. T. Mendonça, Nonlinear Laser Driven Donut Wakefields for Positron and Electron Acceleration, Phys. Rev. Lett. **112**, 215001 (2014).

[4] Z. Lécz, A. Andreev, and A. Seryi, Plasma rotation with circularly polarized laser pulse, Laser Part. Beams **34**, 31 (2016).

[5] R. Nuter, P. Korneev, I. Thiele, and V. Tikhonchuk, Plasma solenoid driven by a laser beam carrying an orbital angular momentum, Phys. Rev. E **98**, 033211 (2018).

[6] J. Vieira, J. T. Mendonça, and F. Quéré, Optical Control of the Topology of Laser-Plasma Accelerators, Phys. Rev. Lett. **121**, 054801 (2018).

[7] J. T. Mendonça, S. Ali, and B. Thidé, Plasmons with orbital angular momentum, Phys. Plasmas **16**, 112103 (2009).

[8] J. T. Mendonça, Kinetic description of electron plasma waves with orbital angular momentum, Phys. Plasmas **19**, 112113 (2012).

[9] Y. Shi, J. Vieira, R. M. G. M. Trines, R. Bingham, B. F. Shen, and R. J. Kingham, Magnetic Field Generation in Plasma Waves Driven by Copropagating Intense Twisted Lasers, Phys. Rev. Lett. **121**, 145002 (2018).

[10] I. S. Gradstein and I. M. Ryzik, in *Table of Integrals, Series, and Products*, 6th ed., edited by A. Jeffrey and D. Zwillinger (Academic Press, Cambridge, 2000).

[11] R. Nuter and V. Tikhonchuk, Prepulse suppression and optimization of backward Raman amplification with a chirped pump laser beam, Phys. Rev. E **87**, 043109 (2013).

[12] A. R. Bell and P. Gibbon, Electron non-linearities in Langmuir waves with application to beat-wave experiments, Plasma Phys. Controlled Fusion **30**, 1319 (1988).

[13] L. Gorbunov, P. Mora, and T. M. Antonsen, Jr., Magnetic Field of a Plasma Wake Driven by a Laser Pulse, Phys. Rev. Lett. **76**, 2495 (1996).

[14] J. D. Jackson, *Classical Electrodynamics* (John Wiley & Sons, New York, 1962).

[15] P. Ramachandran, MAYAVI: A free tool for CFD data visualization, in *Proceedings of the 4th Annual CFD Symposium* (Aeronautical Society of India, New Delhi, 2001).